This article has been accepted for publication in a future issue of this journal, but has not been fully edited. Content may change prior to final publication. Citation information: DOI 10.1109/TVT.2018.2827408, IEEE Transactions on Vehicular Technology



# Multi-Target AOA Estimation using Wideband LFMCW Signal and Two Receiver Antennas

Dongheng Zhang, Ying He, Xinyu Gong, Yang Hu*, Yan Chen, *Senior Member, IEEE,* and Bing Zeng, *Fellow, IEEE*

***Abstract*—Linear frequency modulated continuous wave (LFMCW) signals have been widely used in target detection and localization, thanks to their good detection sensitivity and high range resolution. However, estimation of the angle of arrival (AOA) of the LFMCW signal reflected from each target in a multi-target environment is still quite limited at present. In this paper, we propose a novel AOA estimation framework in which one transmitter antenna and two receiver antennas are employed to transmit a wideband LFMCW signal and receive the signals reflected from different targets, respectively. The signals received at two receiver antennas are processed in three steps. First, each of them is demodulated by mixing with the transmitted signal to transform the wideband non-stationary signal into superposition of a series of single-tone signals. Second, signals received at each receiver antenna from different targets are separated using bandpass filtering. Third, the corresponding AOA of each target is estimated using the phase difference between two receiver antennas. Different from the traditional subspace-based methods, the number of targets is not limited by the number of receiver antennas. The theoretical analysis and simulation results show that the proposed algorithm can achieve accurate AOA estimation for multiple targets even at a low signal to noise ratio.**

***Index Terms*—Angle of arrival, AOA estimation, LFMCW, multi-target detection, time-of-flight (TOF)**

## I. Introduction

TARGET detection and localization has been an active research area due to its importance in a wide range of applications including autonomous vehicle, vital signs detection [1], etc. Linear frequency modulated (LFM) signals are often used in active detection systems due to their good target detection sensitivity of low Doppler targets [2] and high range resolution [3]. As a key component of target detection, angle of arrival (AOA) estimation of LFM signals is of particular importance and has received great attentions, especially with the development of Internet of Things (IoT) in recent years.

The most widely used technique for the AOA estimation is the subspace-based method, where the multiple signal classification (MUSIC) algorithm [4] serves perhaps as the best example. MUSIC generates signal subspaces and noise subspaces from the eigen-decomposition on the autocorrelation matrix and then obtains the AOA estimation via orthogonality between the steering vectors and noise subspaces. To decrease the computational complexity of the MUSIC algorithm, some modified MUSIC algorithms have been proposed in recent years through avoiding the eigen-decomposition or limiting the range for spectral search [5]-[7]. Another well-known subspace-based method is the estimation of signal parameters via rotational invariance techniques (ESPRIT) algorithm [8], which utilizes the rotational invariance property of the signal subspace to accomplish the AOA estimation. The main advantage of the ESPRIT algorithm is that the beam scan is not needed, thus reducing the computational complexity significantly. However, these subspace-based methods are designed for narrow-band stationary signals and therefore cannot be applied directly to the LFM signals because they are non-stationary signals whose instantaneous frequency varies with time. Note that when the source signal is available, the mixed signal between the reflected signal and source signal can be stationary. Nevertheless, the subspace-based methods still cannot be directly used since the frequency of the mixed signal can be very different on different antennas.

To solve the problem, methods that combine the fractional Fourier transform (FRFT) [9] and some conventional subspace-based algorithms have been proposed [10], [11]. It has been found that the LFM signals can be regarded as stationary signals in the fractional Fourier domain by rotating the signal coordinates counterclockwisely, and thus the conventional subspace-based algorithms can be applied. Tao *et al.* proposed to combine FRFT and MUSIC algorithm to estimate the AOA of the wideband LFM signals [12]. However, it is valid only for uncorrelated signals. The AOA estimation for coherent LFM signals was proposed by Qu *et al.* [13], where the forward/backward (FB) spatial smoothing technique is combined with the FRFT technique. However, this method reduced the array aperture, and thus the accuracy was restricted. To avoid reducing the array aperture, Jin *et al.* proposed to combine FRFT with the virtual array transform [14]. An improved ESPRIT algorithm based on FRFT was proposed in [15] for both coherent and non-coherent LFM signals in a complex environment.

Another way to deal with non-stationary signals, especially the narrow-band chirp signals, is the spatial-time-frequency distribution (STFD) technique [16], [17]. The most widely used tool for the spatial-time-frequency analysis is the Wigner Ville distribution (WVD) technique. In [18], a WVD-based



*Corresponding author: Yang Hu (yanghu@uestc.edu.cn).

This work was partly supported by the National Natural Science Foundation of China under Grant 61602090 and 61672137, the 111 Project No. B17008, and the Thousand Youth Talents Program of China (to Yan Chen).

The authors are with School of Information and Communication Engineering, also with Center of Future Media, University of Electronic Science and Technology of China, Chengdu, Sichuan, China, 611731. E-mails: {eedhzhang, YingHe, xy_Gong}@std.uestc.edu.cn, {yanghu, eecyan, eezeng}@uestc.edu.cn

This article has been accepted for publication in a future issue of this journal, but has not been fully edited. Content may change prior to final publication. Citation information: DOI 10.1109/TVT.2018.2827408, IEEE Transactions on Vehicular Technology



method was proposed, which extends the STFD concept to the wideband case. However, this technique requires some preliminary information about the source localization angular sectors or initial direction-of-arrival (DOA) estimates[1], which may lead to a strongly-biased conclusion. Zhang *et al.* proposed a spatial polarimetric time-frequency distributions (SPTFD) algorithm [19], which extends STFD to utilize the source polarization properties. The SPTFD algorithm allows the discrimination of sources based on their respective DOA as well as their polarization and time-frequency signal characteristics. Note that the STFD-based methods suffer from cross-term interference severely in the low signal-to-noise ration (SNR) region under the multi-LFM signal condition, which results in a performance degradation.

Some sophisticated techniques have also been utilized to estimate the AOA. Ma and Goh proposed to use the ambiguity function to convert the absolute time and frequency of the chirp signals into relative time lag and frequency difference, and then use conventional beamforming and MUSIC algorithms to estimate the AOA [20]. However, the performance decreases rapidly in low SNR conditions, especially when the duration of signal is very short. The modal analysis technique was utilized in [21] to generate the focusing matrices for the wideband AOA estimation. It was shown that no prior information except the array geometry is needed, which demonstrates desirable properties and promising capabilities of the modal analysis technique in preprocessing wideband signals that are received at a sensor array. Daegu *et al.* proposed to exploit the dual shift invariant structure in the time and space domains for the AOA estimation [22], according to which the AOA estimation of multiple targets can be achieved with a two-channel frequency modulated continuous wave (FMCW) radar. Generally, methods mentioned above require a large array to guarantee the performance. However, such an array is expensive and may not be available in many scenarios, especially in indoor environments. In addition, when the bandwidth of LFMCW signal is large [1], the data rate of the signal increases rapidly, which makes the computational complexity of most existing methods impractical. Thus, our motivation is to propose an AOA estimation method with only a few number of receiver antennas to achieve satisfactory performance.

In this paper, we propose a novel multi-target AOA estimation framework in which one transmitter antenna and two receiver antennas are employed. Specifically, the transmitter antenna transmits a wideband LFMCW signal. Through propagation and reflection from targets, each receiver antenna receives superposition of a series of attenuated and delayed versions of the transmitted LFMCW signals, which is non-stationary. We then propose to demodulate the received signals by mixing with the transmitted LFMCW signals, which transforms the received non-stationary signals into stationary ones. Next, we separate the signals reflected from different targets through bandpass filtering and estimate the AOA of each target through the least square technique. Theoretic analysis shows that the proposed algorithm can achieve an unbiased estimate with a small variance. Some advantages of our proposed framework are as follows:

- The number of targets of which the AOA can be estimated is not limited by the number of receiver antennas. Two receiver antennas are enough for estimating the AOA of multiple targets.
- There is no upper frequency limit of signal which is usually perplexed for the traditional antenna array design, i.e., the space between antennas do not need to be smaller than the half wavelength.
- The proposed framework can recognize targets even when they are located at the same direction.
- Theoretic analysis and extensive simulation results show that the proposed framework can achieve good performance for estimating the AOAs of multiple targets even when the SNR decreases to -30dB.

The paper is organized as follows. We describe the system model in detail in Section II. The proposed AOA estimation algorithm is presented in Section III. Section IV performs the theoretic analysis of the proposed algorithm. In Section V, we conduct multiple simulations to validate the proposed framework under different settings. Finally, we introduce discussions in Section VI and draw conclusions in Section VII.

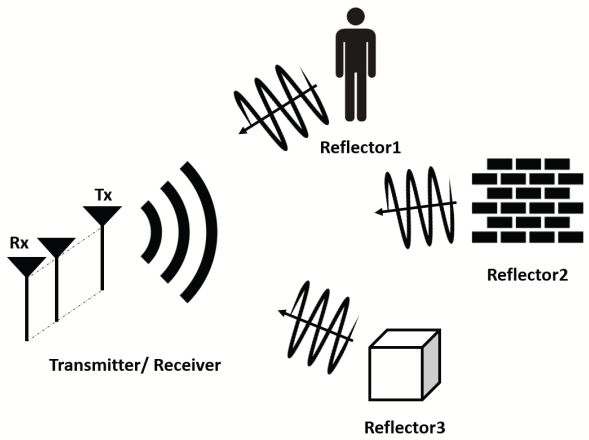


Fig. 1: System model with one transmitter antenna and two receiver antennas.

## II. System Model

We consider a transceiver system with one transmitter antenna and two receiver antennas as shown in Fig. 1. Note that all antennas are mounted on the same device. The transmitter antenna transmits an LFMCW signal and two receiver antennas receive echoes reflected from targets so that the AOAs of distinctive targets are estimated by processing the received echoes.

Let $s(t)$ denote the transmitted LFMCW signal, which can be written as

$$s(t) = A_T e^{j(2\pi f_{min} t + \pi k t^2)}, \quad 0 \le t \le T_{sweep}, \qquad (1)$$

where $A_T$, $f_{min}$, $k$, $T_{sweep}$ denote the amplitude of the signal, the starting frequency of frequency modulation, the frequency

[1]In this paper, we use direction-of-arrival (DOA) and angle-of-arrival (AOA) interchangeably.

This article has been accepted for publication in a future issue of this journal, but has not been fully edited. Content may change prior to final publication. Citation information: DOI 10.1109/TVT.2018.2827408, IEEE Transactions on Vehicular Technology



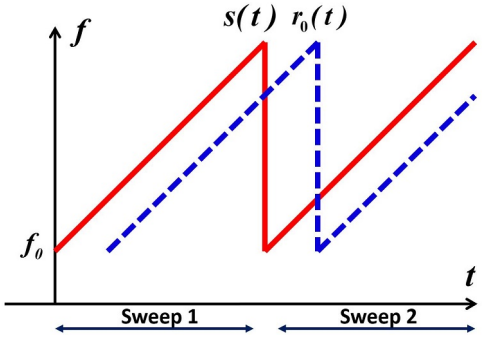


Fig. 2: An illustration of the transmitted signal and reflected signal.

modulated slope, and the time duration of signal, respectively. The instantaneous frequency of the LFMCW signal is

$$f = \frac{1}{2\pi}\frac{\mathbf{d}(2\pi f_{min}t + \pi k t^2)}{\mathbf{d}t} = f_{min} + kt. \tag{2}$$

In our system, the transmitted signal will be received by the receiver after propagation. Suppose that the signal received by the receiver antennas is reflected by a specific reflector. Then, the received signal can be expressed as

$$r_0(t) = A_R e^{j(2\pi f_{min}(t-\tau)+\pi k(t-\tau)^2)}, \tag{3}$$

where $A_R$ and $\tau$ denote the reflected signal amplitude and the time of flight (TOF), respectively. Comparing (1) and (3), we can see that the received signal is a scaled and delayed version of the transmitted signal.

According to [23], the amplitude $A_R$ can be expressed as

$$A_R = A_T \frac{R\sqrt{G_T G_R}}{d(t)^\alpha}, \tag{4}$$

where $R$ denotes the reflection coefficient which is determined by the radar cross section (RCS) of the reflector, $G_T$ and $G_R$ denote the gain of transmitter and receiver antennas, respectively, $d(t)$ denotes the propagation distance from the transmitter to the reflector and back to the receiver, $\alpha$ is the attenuation coefficient which is determined by the environment of propagation.

The time of flight $\tau$ is given by

$$\tau = \frac{d(t)}{c}, \tag{5}$$

where $c$ is the velocity of light in the space.

As shown in Fig. 1, the received signal is the superposition of a series of signals from different reflectors perturbed by the noise of the receiver. Under the assumption that signals scattering and reflecting from unsmooth surface of the same reflector are merged together because of the limited bandwidth, the aggregated signal $r(t)$ can be written as

$$r(t) = \sum_{i=1}^{N} A_{Ri} e^{j(2\pi f_{min}(t-\tau_i)+\pi k(t-\tau_i)^2)} + w(t), \tag{6}$$

where $N$ is the number of reflectors, $i$ denotes the index of the $i^{th}$ path of propagation and $w(t)$ is the zero-mean additive complex white Gaussian noise at the receiver with variance $\sigma_0^2$.

## III. The Proposed AOA Estimation Algorithm

In this section, we describe the proposed AOA estimation algorithm in detail. There are mainly three steps involved in the proposed algorithm. First, the received signal is demodulated by mixing with the transmitted signal to transform the wideband non-stationary signal into superposition of a series of single-tone signals. Second, the number of reflectors is determined using hypothesis tests. Third, signals from different reflectors are separated using bandpass filtering and the corresponding AOA of each reflector is estimated using the phase difference between two receiver antennas.

### A. Preprocessing of the received signal

LFMCW signal is a wideband non-stationary signal. Compared to the transmitted signal, the received signal is attenuated on amplitude and delayed in time. The frequency relation between the transmitted signal and received signal is shown in Fig. 2. By utilizing the time delay characteristic of the received signal, we can mix the received signal with the transmitted signal to extract the information about the reflector. Specifically, the mixed signal can be written as

$$\begin{aligned} s_d(t) = s(t)r^*(t) = \sum_{i=1}^{N} A_T A_{Ri} e^{j(2\pi f_{min}\tau_i + 2\pi k t\tau_i - \pi k\tau_i^2)} \\ + A_T e^{j(2\pi f_{min}t + \pi k t^2)} w^*(t). \end{aligned} \tag{7}$$

The first part in (7) corresponds to the signal that is the superposition of a series of single-tone signals from different reflectors. In this paper, we assume that the distances of reflectors are different. The frequency of this signal corresponds to the TOF, which is determined by the distance from the transmitter to a reflector and back to the receiver. In other words, the signals reflected from a specific distance have the same frequency and the signals reflected from different distances have different frequencies [24][25]. Note that although the Doppler shift will affect the frequency of the received signal, when the frequency slope of the LFMCW signal is high, the effect of the Doppler shift is negligible. In such a case, bandpass filter can be used to separate the signals from reflectors at different distances. The second part in (7) corresponds to the cross-term of signal and noise. The mixing process transforms the wideband non-stationary signals into stationary signals with a single frequency, due to which we can use classic signal processing techniques such as DFT to extract the information of the signal.

In practice, the received signal is sampled by an A/D converter to obtain its discrete version as follows:

$$\begin{aligned} s_d(mT_s) = \sum_{i=1}^{N} A_T A_{Ri} e^{j(2\pi f_{min}\tau_i + 2\pi k m T_s\tau_i - \pi k\tau_i^2)} \\ + A_T e^{j(2\pi f_{min}mT_s + \pi k(mT_s)^2)} w^*(mT_s), \end{aligned} \tag{8}$$

where $T_s$ denotes the sampling interval.

### B. Determining the number of reflectors

The number of reflectors is an essential prior information for the AOA estimation. According to (8), the received signal

This article has been accepted for publication in a future issue of this journal, but has not been fully edited. Content may change prior to final publication. Citation information: DOI 10.1109/TVT.2018.2827408, IEEE Transactions on Vehicular Technology



after mixing is a series of single-tone signals with different frequencies, which correspond to the distances between the transceiver and reflectors. By assuming that different reflectors have different distances[2], the number of reflectors can be estimated in the frequency domain. To this end, we perform DFT over one period of the frequency sweep and then use some hypothesis tests to determine the number of reflectors. According to (8), the mixed signal can be divided into two parts as follows

$$s_d(mT_s) = y(mT_s) + z(mT_s), \tag{9}$$

where

$$y(mT_s) = \sum_{i=1}^{N} A_T A_{Ri} e^{j(2\pi f_{\min}\tau_i + 2\pi k m T_s \tau_i - \pi k {\tau_i}^2)}, \tag{10}$$

and

$$z(mT_s) = A_T e^{j(2\pi f_{\min} m T_s + \pi k (mT_s)^2)} w^*(mT_s). \tag{11}$$

With the linearity of DFT, we can perform DFT on two parts separately. The DFT of $y(m)$ is given by

$$\begin{aligned} Y[k] &= \sum_{m=1}^{M} y(m) e^{-j\frac{2\pi}{M}km} = \sum_{m=1}^{M}\sum_{i=1}^{N} A_T A_{Ri} e^{i\phi_{\mathrm{y}}^{im}}, \\ &= \sum_{m=1}^{M}\sum_{i=1}^{N} A_T A_{Ri}(\cos\phi_{\mathrm{y}}^{im} + j\sin\phi_{\mathrm{y}}^{im}), \end{aligned} \tag{12}$$

with $\phi_{\mathrm{y}}^{im}$ being defined as

$$\phi_{\mathrm{y}}^{im} = 2\pi f_{\min}\tau_i + 2\pi k T_s \tau_i m - \pi k {\tau_i}^2 - 2\pi k m/M.$$

The $w(mT_S)$ is assumed to be a white complex Gaussian noise, which can be written as

$$w(mT_S) = w_R(mT_S) + j w_I(mT_S), \tag{13}$$

where $w_R$ and $w_I$ are independent Gaussian noise. The DFT of $z(mT_S)$ can thus be expressed as

$$\begin{aligned} Z[k] &= \sum_{m=1}^{M} [w_R(mT_s) A_T e^{j\varphi_{\mathrm{z}}^m} + j w_I(mT_s) A_T e^{j\varphi_{\mathrm{z}}^m}], \\ &= \sum_{m=1}^{M} [w_R(mT_s) A_T \cos(\varphi_{\mathrm{z}}^m) - w_I(mT_s) A_T \sin(\varphi_{\mathrm{z}}^m)] \\ &+ j\sum_{m=1}^{M} [w_R(mT_s) A_T sin(\varphi_{\mathrm{z}}^m) + w_I(mT_s) A_T cos(\varphi_{\mathrm{z}}^m)], \end{aligned} \tag{14}$$

with $\varphi_{\mathrm{z}}^m$ being defined as

$$\varphi_{\mathrm{z}}^m = 2\pi f_{\min} m T_s + \pi k (mT_s)^2 - 2\pi k m/M. \tag{15}$$

The DFT $S_d[k]$ of the signal $s_d(mT_S)$ is superposition of the DFTs of $y(mT_S)$ and $z(mT_S)$ as follows

$$S_{\mathrm{d}}[k] = Y[k] + Z[k]. \tag{16}$$

[2]In this paper, we use reflector and target interchangeably.

**Algorithm 1** Determining the number of reflectors

1: Estimate the noise variance $\sigma^2$
2: Mix the received signal $r(m)$ with the transmitted $s(m)$ signal
3: Perform FFT on one duration $T_{sweep}$ of the mixed signal $s_d(t)$
4: Calculate the conditional probability $p(A|H_0)$ and $p(A|H_1)$
5: Determine the optimal threshold $\eta_0$
6: Estimate the number of reflectors using $\eta_0$ and $L(A)$

Then, let us define $H_0$ and $H_1$ as the hypothesis that there is no reflector and the hypothesis that there is a reflector, respectively, as below

$$\begin{aligned} H_0: &\quad A[k] = |S_d[k]| = |Z[k]|, \\ H_1: &\quad A[k] = |S_d[k]| = |Y[k] + Z[k]|. \end{aligned} \tag{17}$$

Then, a threshold detector can be designed, where the performance can be described using the probability of detection $P_D$ and probability of false alarm $P_F$ defined as

$$\begin{aligned} P_D &= P(A[k] > A_0|H_1), \\ P_F &= P(A[k] > A_0|H_0). \end{aligned} \tag{18}$$

where $A_0$ is the threshold.

According to the expression of $Z[k]$ in (14), the real and imaginary parts of $Z[k]$ are the superposition of $M$ identical independent Gaussian variables with zero mean and variance $\sigma^2$. Thus, the real and imaginary parts of $Z[k]$ obeys Gaussian distribution with zero mean and variance $M\sigma^2$. As such, the amplitude of $Z[k]$ obeys Raleigh distribution as

$$p(A[k]|H_0) = \frac{1}{2MA_T^2\sigma^2} e^{\frac{-A[k]}{2MA_T^2\sigma^2}}. \tag{19}$$

According to (12), (14), and (16), $S_d[k]$ is the superposition of a determined signal $Y[k]$ and random noise $Z[k]$. Therefore, the real and imaginary parts of $S_d[k]$ obey Gaussian distribution with the same variance but different means. In such a case, the amplitude of $S_d[k]$ obeys Rice distribution as [26]

$$p(A[k]|H_1) = \frac{A[k] e^{-\frac{A^2+\mu^2}{2MA_T^2\sigma^2}}}{MA_T^2\sigma^2} I_0\left(\frac{A[k]\mu}{MA_T^2\sigma^2}\right). \tag{20}$$

where $I_0$ denotes the modified Bessel function of zero order and $\mu$ the expectation of the square root of the real and imaginary parts of $Z[k]$.

To determine the number of reflectors without the prior information of $H_1$ and $H_0$, Neyman-Pearson criterion is used. Specifically, the likelihood ratio function can be expressed as

$$L(A[k]) = \frac{p(A[k]|H_1)}{p(A[k]|H_0)}, \tag{21}$$

where $L(A[k])$ is compared with a threshold $\eta_0$ which is determined by false alarm probability $P_F$ to determine the hypothesis.

This article has been accepted for publication in a future issue of this journal, but has not been fully edited. Content may change prior to final publication. Citation information: DOI 10.1109/TVT.2018.2827408, IEEE Transactions on Vehicular Technology



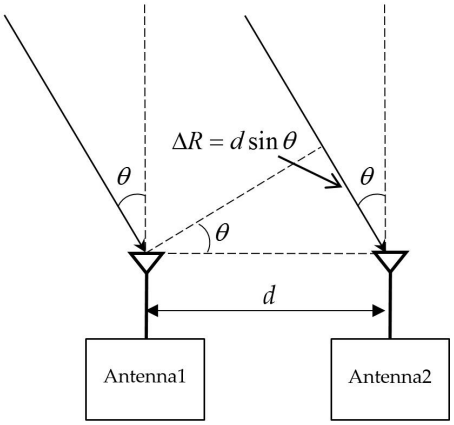


Fig. 3: The structures of the two receiver antennas

### C. Estimating the AOA

After determining the number of the reflectors, the signal from a specific reflector can be separated through bandpass filtering. In this section, to simplify the analysis, we assume that an ideal bandpass filter is performed, i.e., it does not affect the amplitude and phase of the signal. The effects of a practical filter will be discussed in detail in the simulation section.

As shown in Fig. 3, we only use two receiver antennas to estimate the AOA. This is different from the traditional methods that generally require the number of receiver antennas to be greater than the number of reflectors. According to the geometric relation shown in Fig. 3, the TOF of the signal from the same reflector on two receiver antennas is different. Thus, the signal obtained after bandpass filtering can be expressed as

$$\begin{aligned} s_{1d}(t) &= A_T A_{Ri} e^{j(2\pi f_{min}\tau_{1i} + 2\pi k t \tau_{1i} - \pi k \tau_{1i}^2)} + n_1(t), \\ s_{2d}(t) &= A_T A_{Ri} e^{j(2\pi f_{min}\tau_{2i} + 2\pi k t \tau_{2i} - \pi k \tau_{2i}^2)} + n_2(t), \end{aligned} \tag{22}$$

where $\tau_{1i}$ and $\tau_{2i}$ denote the TOF of the signal for two receiver antennas from the $i^{th}$ reflector, $n_1(t)$ and $n_2(t)$ denote the white Gaussian noise after bandpass filtering.

The complex white Gaussian noise $w(t)$ at the receiver is assumed to distribute uniformly in the frequency domain. The bandwidth of Gaussian noise after filtering is determined by the bandwidth of the filter, and thus the relation between $w(t)$ and $n(t)$ is given by

$$\begin{aligned} E[n(t)] &= E[w(t)] = 0, \\ D[n(t)] &= \frac{D[w(t)]}{W}, \end{aligned} \tag{23}$$

where $W$ is the bandwidth of the bandpass filter which is used for filtering the signal from a specific reflector. $E[n(t)]$ and $D[n(t)]$ denote the mean and variance of the noise, respectively.

According to (22), the difference between the phases of the filtered signal on two receiver antennas can be written as

$$\begin{aligned} \psi(t) &= 2\pi f_{min}(\tau_{2i} - \tau_{1i}) + 2\pi k t(\tau_{2i} - \tau_{1i}) \\ &\quad -\pi k(\tau_{2i}^2 - \tau_{1i}^2) + v_2(t) - v_1(t), \end{aligned} \tag{24}$$

where $v_2(t)$ and $v_1(t)$ denote the phase noise. The properties of $v(t)$ will be discussed in detail in next section.

According to the geometric relation of two receiver antennas shown in Fig.3, we have

$$\tau_2 - \tau_1 = \frac{dsin\theta}{c}. \tag{25}$$

Substitute (25) into (24), $\psi(t)$ can be re-written as

$$\begin{aligned} \psi(t) &= 2\pi k \frac{dsin\theta}{c} t + 2\pi f_{min} \frac{dsin\theta}{c} \\ &\quad -\pi k \frac{dsin\theta}{c}(\frac{dsin\theta}{c} + 2\tau_{1i}) + v_2(t) - v_1(t). \end{aligned} \tag{26}$$

In the absence of the noise, $\phi(t)$ is linear in time $t$, and the slope is given by

$$k_\psi = 2\pi k \frac{dsin\theta}{c}. \tag{27}$$

From (27), we can see that $k_\psi$ is a function of $\sin\theta$, which means that we can use $k_\phi$ to obtain $\theta$. This is because the frequency of the received signal is a linear function of the TOF, and the frequencies of the signals from the same reflector on two receiver antennas are different, which make the phase difference be a linear function of time $t$. The frequency difference is determined by the TOF difference of the signal on two receiver antennas which is a linear function of $\sin\theta$. As a result, the slope of phase difference is a function of $\theta$.

With (27), the AOA can be estimated as

$$\theta = arcsin(\frac{k_\psi c}{2\pi k d}). \tag{28}$$

In practice, with the presence of noise, $\phi(t)$ is not strictly linear in $t$. To extract $k_\psi$ from the phase difference which is perturbed by noise, we use the least square method to fit the phase difference. According to (26), the phase difference in the discrete form is given by

$$\begin{aligned} \psi[n] &= 2\pi k \frac{dsin\theta}{c} n T_s + 2\pi f_{min} \frac{dsin\theta}{c} \\ &\quad - \pi k \frac{dsin\theta}{c}(\frac{dsin\theta}{c} + 2\tau_{1i}) + v_2[n] - v_1[n]. \end{aligned} \tag{29}$$

With (29), the least square estimate of $k_\psi$ can be derived as

$$k_\psi = \frac{N(\sum_{i=1}^{N} t_i \psi[i]) - (\sum_{i=1}^{N} t_i \sum_{i=1}^{N} \psi[i])}{N(\sum_{i=1}^{N} t_i{}^2) - (\sum_{i=1}^{N} t_i)^2}, \tag{30}$$

where $t_i = iT_s$, $t_N = NT_s = T_{sweep}$, $T_s$ is the sampling period, and $T_{sweep}$ is the sweep duration of the LFMCW signal.

## IV. Performance Analysis

In the proposed method, targets are assumed to be located with different distances. Thus, signal from different targets can be separated using bandpass filtering. According to [27], the range resolution can be expressed as

$$Range\ Resolution = \frac{c}{2B}, \tag{31}$$

where $B$ and $c$ denote the bandwidth of the transmitted LFMCW signal and the speed of the light, respectively. Note

This article has been accepted for publication in a future issue of this journal, but has not been fully edited. Content may change prior to final publication. Citation information: DOI 10.1109/TVT.2018.2827408, IEEE Transactions on Vehicular Technology



**Algorithm 2** Estimation the AOA

1: Load the number of reflectors and the corresponding center frequency
2: Determine parameters of the bandpass filter and filter the corresponding signals on the two antennas
3: Subtract the angle of the signals on the two antennas
4: Fit the $\psi$ using the least square method
5: Estimate the AOA using equation (29)
6: Repeat 2 until AOA of all reflectors has been estimated

that the bandwidth $W$ in section III denotes the bandwidth of the bandpass filter, which is much smaller than $B$. To separate signal from different targets, the distance difference of targets should be larger than the range resolution.

To derive the mean and variance of $k_\phi$, we simplify the expression of (30) as follows

$$k_\psi = \frac{\sum_{i=1}^{N} \psi[i](Nt_i - \sum_{j=1}^{N} t_j)}{N(\sum_{i=1}^{N} t_i{}^2) - (\sum_{i=1}^{N} t_i)^2}. \tag{32}$$

According to the above equation, the expectation and variance of $k_\phi$ can be obtained as

$$E(k_\psi) = \frac{\sum_{i=1}^{N} E[\psi[i]](Nt_i - \sum_{j=1}^{N} t_j)}{N(\sum_{i=1}^{N} t_i{}^2) - (\sum_{i=1}^{N} t_i)^2}, \tag{33}$$

and

$$D(k_\psi) = \frac{\sum_{i=1}^{N} D[\psi[i]](Nt_i - \sum_{j=1}^{N} t_j)^2}{\left[N(\sum_{i=1}^{N} t_i^2) - (\sum_{i=1}^{N} t_i)^2\right]^2}. \tag{34}$$

To compute $E(\psi[i])$ and $D(\psi[i])$ in (33) and (34), we first derive the probability density function of $\psi[i]$. Let us define $\Omega$ as

$$\Omega = \rho - \rho\sin\theta - \rho\cos(\phi - \psi)\cos\theta, \tag{35}$$

where $\phi$ is the ideal phase difference in the absence of noise, $\psi$ is the actual phase difference in the presence of noise as in (29), $\rho = (A_{Rl}A_{Tl})^2/\sigma_l^2$ is the signal to noise ratio after bandpass filtering, $A_{Rl}A_{Tl}$ is the amplitude of mixed signal after bandpass filtering, and $\sigma_l^2$ is the power of narrow band Gaussian noise.

According to (23), $\rho$ is determined by the signal to noise ratio of the receiver and the bandwidth of the bandpass filter, which can be written as

$$\rho = \frac{SNR \cdot f_s}{W}, \tag{36}$$

where SNR denotes the signal to noise ratio at the receiver, $W$ is the bandwidth of the filter, and $f_s$ is the sampling rate of received signal.

Then, according to [28], the probability density function of $\psi[i]$ is

$$p(\psi[i]) = \frac{1}{4\pi}\int_{-\pi/2}^{\pi/2} e^{-\Omega}(1 + 2\rho - \Omega)\cos\theta d\theta. \tag{37}$$

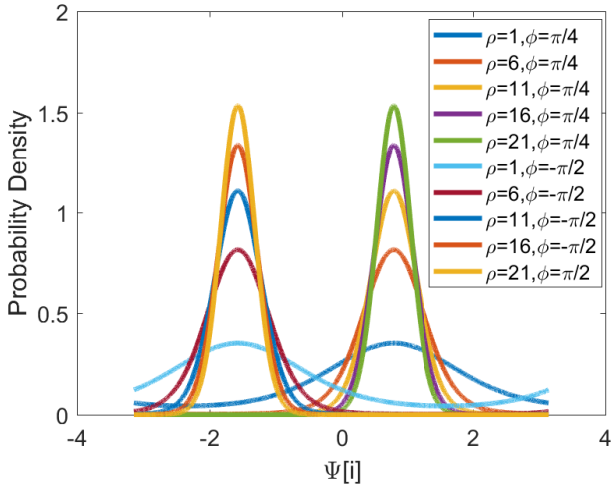


Fig. 4: The probability function of $\psi[i]$ when $\phi = \pi/4$ and $\phi = -\pi/2$

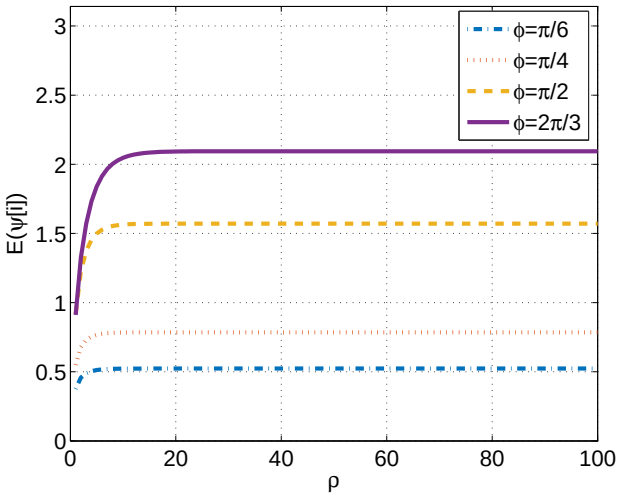


Fig. 5: $E(\psi[i])$ versus $\rho$ under different $\phi$ values.

The integration in (37) is generally difficult to compute, due to which there is no closed-form expression of $E(\psi[i])$ and $D(\psi[i])$. Nevertheless, when $\rho$ and $\phi$ are given, the integration in (37) can be calculated numerically and thus $E(\psi[i])$ and $D(\psi[i])$ can be derived. The probability density function of $\psi[i]$ when $\phi = \pi/4$ and $\phi = -\pi/2$ is shown in Fig. 4. It can be seen from the figure that $\psi[i]$ will be more concentrated around $\phi$ with the increase of $\rho$. We also illustrate in Fig. 5 the relationship between $E[\psi]$ and $\rho$ when $\phi = \pi/6$, $\pi/4$, $\pi/2$ and $2\pi/3$, respectively. It can be seen from the figure that $E(\psi[i])$ approaches to $\phi$ with the increase of $\rho$. According to (36), the value of $\rho$ is usually large as the bandwidth of the bandpass filter is typically small. Therefore, $E(\psi[i])$ is generally an unbiased estimation of $\phi$, and thus $k_\phi$ is also an unbiased estimation.

According to the central limit theorem, $k_\phi$ can be approximated as a Gaussian distribution. Fig. 6 shows the relationship between $D(\psi[i])$ and $\rho$ when $\phi = \pi/6$, $\pi/4$, $\pi/2$ and $2\pi/3$,

This article has been accepted for publication in a future issue of this journal, but has not been fully edited. Content may change prior to final publication. Citation information: DOI 10.1109/TVT.2018.2827408, IEEE Transactions on Vehicular Technology



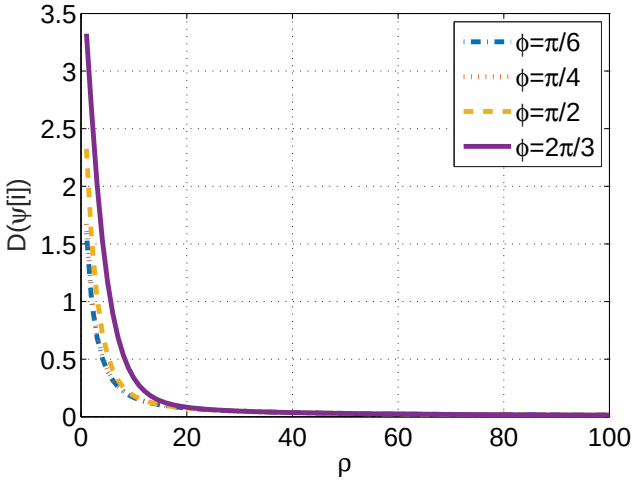


Fig. 6: $D(\psi[i])$ versus $\rho$ under different $\phi$ values.

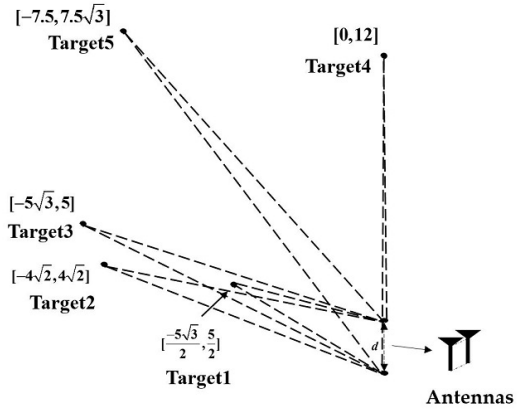


Fig. 7: The locations of different targets.

respectively. It can be seen from the figure that $D(\psi[i])$ approaches to zero with the increase of $\rho$. Fig. 6 also shows that when $\rho$ is large, $D(\psi[i])$ can be approximated as a constant even for different $\phi$. Since $\rho$ is generally large, we approximate $D(\psi[i])$ as a constant $D(\psi[i]) = D_\psi$ for all $i$. Then, the variance of $k_\phi$ can be expressed as

$$D[k_\phi] = \frac{D_\psi \sum_{i=1}^{N} (Nt_i - \sum_{j=1}^{N} t_j)^2}{\left[N(\sum_{i=1}^{N} t_i^2) - (\sum_{i=1}^{N} t_i)^2\right]^2}. \quad (38)$$

According to (38), we can see that $D[k_\psi]$ is a decreasing function of the number of samples $N$. Thus, we can increase the sampling rate to improve the accuracy the estimation. From the discussions above, it can be seen that the estimation accuracy is determined by two factors: the signal to noise ratio after bandpass filtering, $\rho$, which is determined by the SNR of the receiver and the bandwidth of the bandpass filter, and the number of samples $N$. With the increase of $\rho$ and/or $N$, the estimation accuracy can be improved.

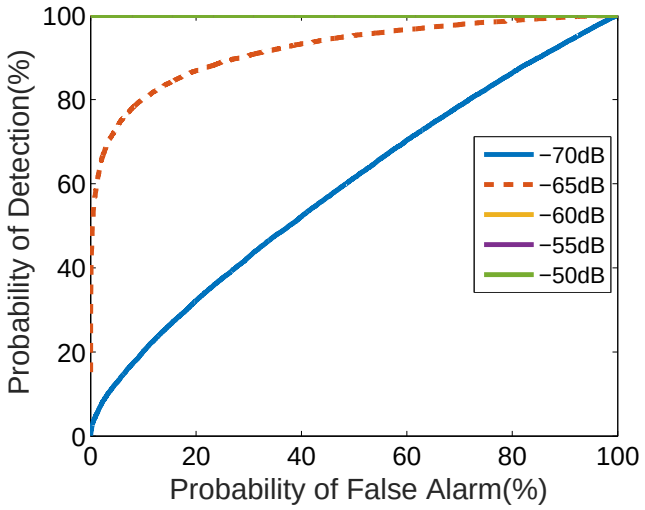


Fig. 8: The ROC curve of determining the number of reflector

## V. Numerical Simulations

In this section, we conduct a series of simulations to validate the effectiveness of the proposed algorithm. The starting frequency $f_{min}$ and the period of the signal $T_{sweep}$ are set to be 5GHz and 2.5ms, respectively. The signal is received by two parallel antennas with spacing of $0.04m$. The signal to noise ratio at the receiver antenna is defined as $SNR = A_R^2/\sigma_0^2$. The performance of estimation is evaluated using the root mean square error (RMSE) defined as

$$RMSE = \sqrt{\frac{1}{L}\sum_{i=1}^{L} |\hat{\theta} - \theta)|^2}, \quad (39)$$

where $\hat{\theta}$ denotes the estimated value of AOA and $\theta$ is the true value of AOA. Some of the locations of targets in our simulations are shown in Fig. 7. Two receiver antennas are assumed to locate in [0,0]m and [0,-0.04]m, respectively. Targets distribute in the second quadrant so that $\theta$ varies from 0 to $\pi/2$.

### A. Determining the number of targets

To verify the effectiveness of the algorithm proposed in Section III which determines the number of targets, the probability of false alarm $P_F$ and the probability of detection $P_D$ is calculated, and the ROC curve, i.e., $P_d$ versus $P_{fa}$, for SNR varying from -70dB to -50dB with stepsize of 5dB is plotted in Fig. 8. As shown in the figure, the proposed method has a good performance even with very low SNR.

### B. Single target with bandwidth 1.5GHz

In this subsection, we consider single target scenario, where the target locates at $[-2.5\sqrt{3}, 2.5]$m. The SNR is assumed to vary from -30dB to 30dB with a stepsize of 5dB. According to the discussions in section III, the frequency of the mixed received signal is proportional to the distance of the reflector. Since the distance of reflector $d(t)$ is smaller than 17.5m in

This article has been accepted for publication in a future issue of this journal, but has not been fully edited. Content may change prior to final publication. Citation information: DOI 10.1109/TVT.2018.2827408, IEEE Transactions on Vehicular Technology



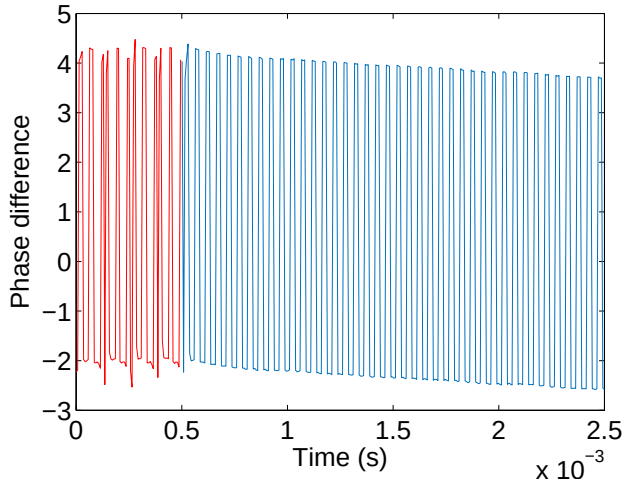


Fig. 9: The phase difference after bandpass filtering.

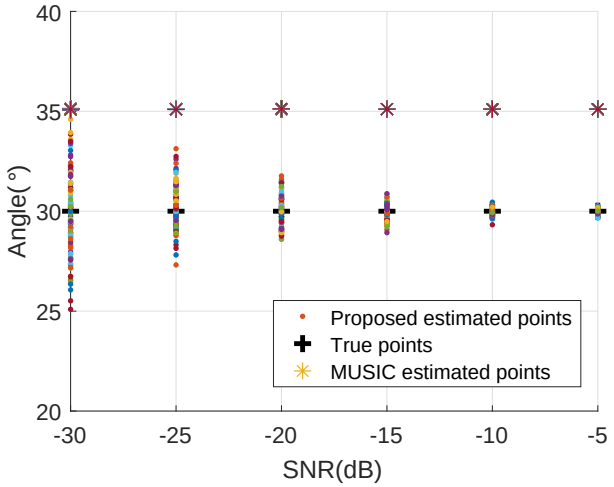


Fig. 11: Distribution of the estimated AOA using MUSIC and proposed algorithm.

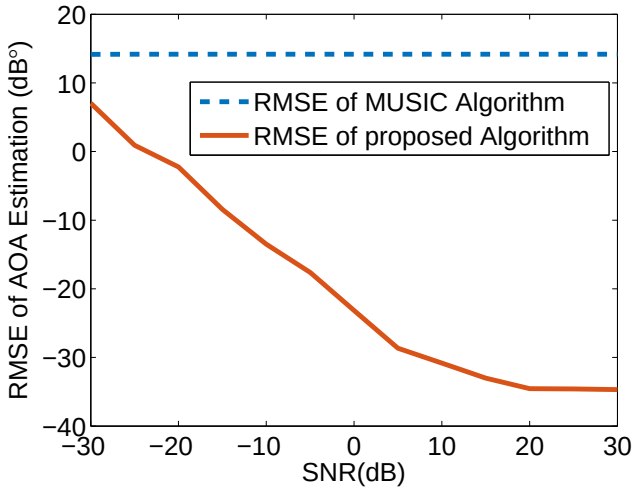


Fig. 10: RMSE of MUSIC algorithm and proposed algorithm.

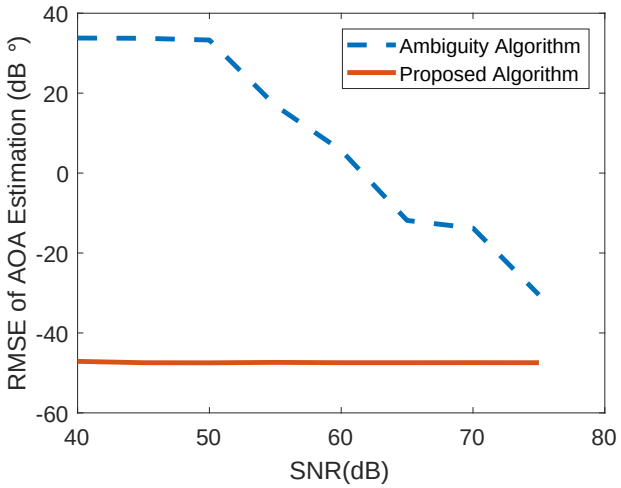


Fig. 12: RMSE of proposed algorithm and Ambiguity based algorithm[20].

this case, the sampling rate of the mixed received signal is set to be 140kHz which can satisfy the Nyquist sampling criteria. The signal is filtered using an FIR bandpass filter with the pass-bandwidth of 4kHz.

In our theoretic derivation, we assume that the bandpass filter is ideal which will not affect the phase difference of the signal. However, $\psi[i]$ will be perturbed by the practical filter in the filtering process. Fig. 9 shows the phase difference of the signal on the two receiver antennas. It can be seen that approximately 1/5 of the data is perturbed which is marked with red. To ensure the accuracy of the least square fitting, we only use the rest part of the data to fit $k_\psi$. The length of the perturbed data is determined by the order of the filter, which is known.

From Fig. 9, we can see that the phase difference oscillates among $[-2\pi, 2\pi]$ which is not consistent with our theoretical analysis. That is because (24) is the unwrapped phase difference of the signal on the two receiver antennas. The phase of each signal lies in $[-\pi, \pi]$ in practice. As a result, $\psi[i]$ lies in $[-2\pi, 2\pi]$. In general, $\psi$ can be expressed as

$$\begin{aligned}\psi[i] &= (2\pi f_{min}\tau_{1i} + 2\pi k t\tau_{1i} - \pi k\tau_{1i}^2)\ mod\ (2\pi) \\ &- (2\pi f_{min}\tau_{2i} + 2\pi k t\tau_{2i} - \pi k\tau_{2i}^2)\ mod\ (2\pi). \quad (40)\end{aligned}$$

Due to the $mod(2\pi)$ operation, the value of $\psi[i]$ oscillates. However, we can see from Fig. 9 that the slope of $\psi[i]$ is not affected. Therefore, we divide the data into two parts based on whether it is greater than 0 or not, and then fit each part using least square method to estimate the slope. Finally, we average the result to determine $k_\psi$. It can be seen from the Fig. 10 that the proposed algorithm can achieve very high accuracy even when SNR drops to -30dB.

According to (7), the mixed signal is the superposition of a series of single-tone signals. As a result, it seems that AOA of the mixed signal can be estimated using traditional methods such as MUSIC. However, due to the linear-frequency characteristic of LFMCW signal, according to (7), the mixed signals on two receiver antennas are different, which makes an

This article has been accepted for publication in a future issue of this journal, but has not been fully edited. Content may change prior to final publication. Citation information: DOI 10.1109/TVT.2018.2827408, IEEE Transactions on Vehicular Technology



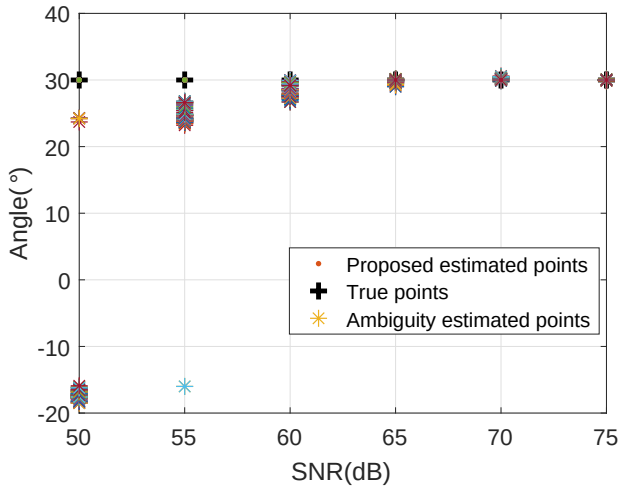


Fig. 13: Distribution of the estimated AOA using proposed algorithm and Ambiguity based algorithm[20].

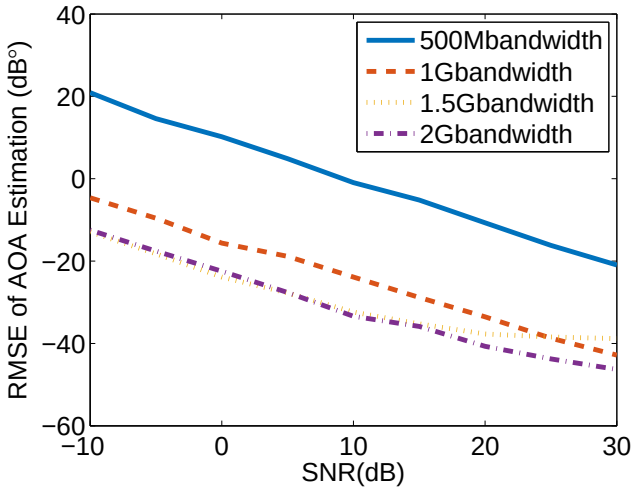


Fig. 14: RMSE for one target located at 5m away with different bandwidth.

estimation bias when using the MUSIC algorithm. Thus, we first compare the proposed method with the MUSIC algorithm. A uniform 8 antennas linear array with an internal spacing of 0.04m is used for the MUSIC algorithm. The performance comparison is shown in Fig. 10. The estimated AOA of the proposed method and the MUSIC algorithm is shown in Fig. 11. We can see that the proposed method can achieve good performance even with very low SNR, and the performance improves as the SNR increases. With 8 antennas, the MUSIC algorithm can achieve robust estimation even when SNR drops to -30dB, however, the estimation error of the MUSIC algorithm is about $5^\circ$ even with a high SNR, which is caused by the frequency difference of signals on different antennas.

We then compare the performance of the proposed method with the incoherent wideband chirp DOA estimation (BCD-I) in [20], which is based on the ambiguity function and MUSIC algorithm. The RMSE of two methods are shown in Fig. 12. The estimated AOA of the proposed method and the ambiguity function based method is shown in Fig. 13 We can see that the ambiguity function based method can achieve high accuracy only when SNR is very high. When SNR is lower than 60dB, the performance degrades rapidly. That is because the average output SNR of ambiguity function is given by [20]

$$\mathrm{SNR}_{\mathrm{am}} \approx \frac{T_{sweep}}{2} \frac{\mathrm{SNR}_0^2}{2\mathrm{SNR}_0 + 1}, \tag{41}$$

where $\mathrm{SNR}_0$ denotes the SNR of the received signal.

From (41), we can see that the $\mathrm{SNR}_{\mathrm{am}}$ is determined by $T_{sweep}$ and $\mathrm{SNR}_0$. With a very small $T_{sweep}$ in our case, the method in [20] requires very high $\mathrm{SNR}_0$ to achieve accurate AOA estimation. That is mainly because the method based on ambiguity function is designed for sonar signal processing, of which the $T_{sweep}$ is much larger. Thus, although we have verified the effectiveness of the ambiguity function based method when using parameters for sonar systems, it is not suitable for microwave signal. On the other hand, with the proposed method, the AOA estimation can be very accurate even at very low SNR region.

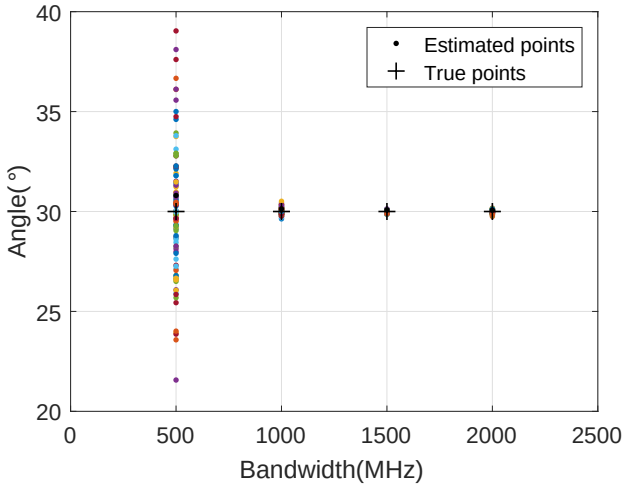


Fig. 15: Distribution of the estimated AOA for one target located at 5m away when the SNR is 0dB.

### *C. Single target with bandwidth varying from 500MHz to 2GHz*

To evaluate the performance of the proposed algorithm under different bandwidth, we conduct simulations using different bandwidth with the same sweep time. The target is assumed to locate at $[-2.5\sqrt{3}, 2.5]$m, while the bandwidth of signal is set to be 500MHz, 1GHz, 1.5GHz, and 2GHz respectively. The SNR varies from -10dB to 30dB with a stepsize of 5dB.

The RMSE performance of the estimation is shown in Fig. 14. From the figure, we can observe that the RMSE decreases as the bandwidth increases. With 500MHz bandwidth, the RMSE is smaller than 3 degree when the SNR=0dB, and the RMSE reduces to below 1 degree when the SNR=10dB. As the bandwidth increases, the RMSE is smaller than 1 degree even when the SNR=-10dB, which shows the effectiveness of the proposed algorithm. The distribution of the estimated points and trues points is illustrated in Fig. 15. The figure shows that

This article has been accepted for publication in a future issue of this journal, but has not been fully edited. Content may change prior to final publication. Citation information: DOI 10.1109/TVT.2018.2827408, IEEE Transactions on Vehicular Technology



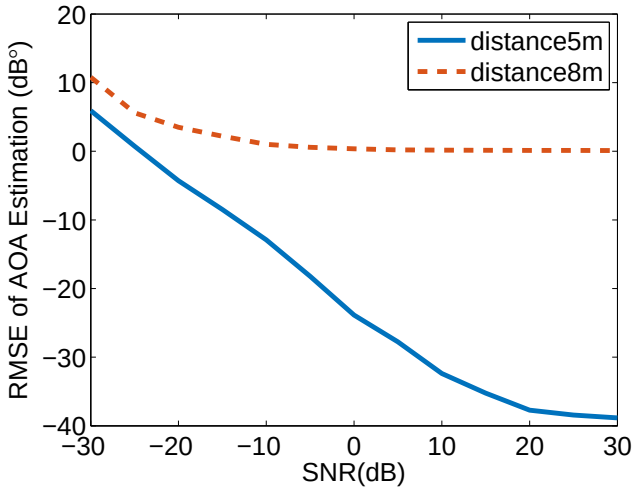


Fig. 16: RMSE of Case I where two targets located at 5m away and 8m away, respectively.

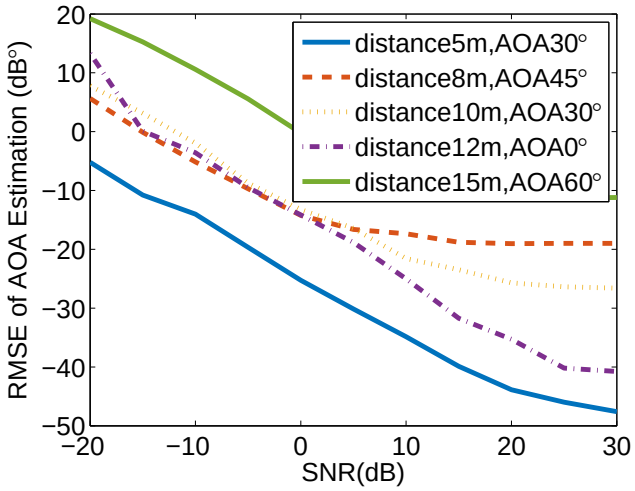


Fig. 17: RMSE of Case II.

the estimated points have larger deviation when the bandwidth is small. It is because when bandwidth is low, the frequency difference of the mixed received signal is small. As a result, the slope of the phase difference would be too small and thus easy to be perturbed by the noise.

### *D. Multiple targets with bandwidth 1.5GHz*

Different from the subspace-based methods, the capability of the proposed algorithm in detecting the number of targets is not limited by the number of receiver antennas. To validate capability of the proposed algorithm in estimating the AOA for multiple targets simultaneously, we conduct simulations under the following three settings:

*1) Case I:* Two targets locate at $[-2.5\sqrt{3}, 2.5]$m and $[-4\sqrt{2}, 4\sqrt{2}]$m, respectively.

*2) Case II:* Five targets locate at $[-2.5\sqrt{3}, 2.5]$m, $[-4\sqrt{2}, 4\sqrt{2}]$m $[-5\sqrt{3}, 5]$m, $[0, 12]$m, and $[-7.5, 7.5\sqrt{3}]$m, respectively.

*3) Case III:* Two targets locate at $[22.5\sqrt{3}, 22.5]$m and $[25\sqrt{2}, 25\sqrt{2}]$m, respectively.

The RMSE performance of Case I is shown in Fig. 16. It can be seen from the figure that the AOA estimation of the target closer to the transmitter has higher accuracy than that of the further one. This is mainly because the power of signal from the closer one is much larger than that of the further one. As a result, signals from the further one are affected more significantly by noise than the closer one, which decreases the accuracy of the AOA estimation.

The results of Case II where the AOA of five different targets are estimated simultaneously are illustrated in Fig. 17. The figure shows that even with only two receiver antennas, the proposed algorithm can still have very high estimation accuracy for all five targets. With 0dB SNR, the RMSE of all five targets is smaller than 1 degree. Also, the estimation accuracy of further targets is again lower than those of closer ones. The corresponding distribution of the estimation is illustrated in Fig. 18. We can see that the estimation for the furthest target deviates much greater than other targets.

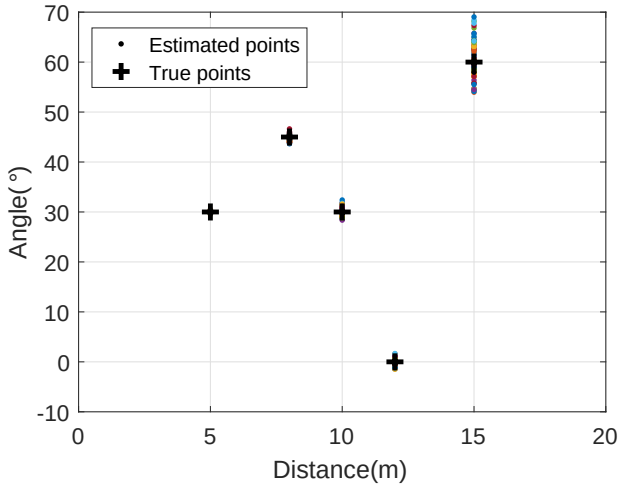


Fig. 18: Distribution of AOA estimation for Case II when SNR is -10dB.

For all simulations discussed above, targets are considered to be located in near field. In Case III, we consider the scenario where two targets are located in far field with distance of 45m and 50m to the transmitter, respectively. The results are shown in Fig. 19. We can see that even with the far field scenario, the proposed algorithm can still achieve high estimation accuracy for both targets.

### *E. The impact of the number of antennas*

The proposed method can achieve accurate AOA estimation using only two receiver antennas. Similar to traditional methods, we can further improve the performance of the proposed method by increasing the number of receiver antennas. To verify the effectiveness of the proposed method, we increase the number of receiver antennas and the performance is shown in Fig. 20. The estimated AOA using multiple receiver antennas is the average of estimation of the pairs of adjacent receiver antennas in the array. As shown in the figure, the

This article has been accepted for publication in a future issue of this journal, but has not been fully edited. Content may change prior to final publication. Citation information: DOI 10.1109/TVT.2018.2827408, IEEE Transactions on Vehicular Technology



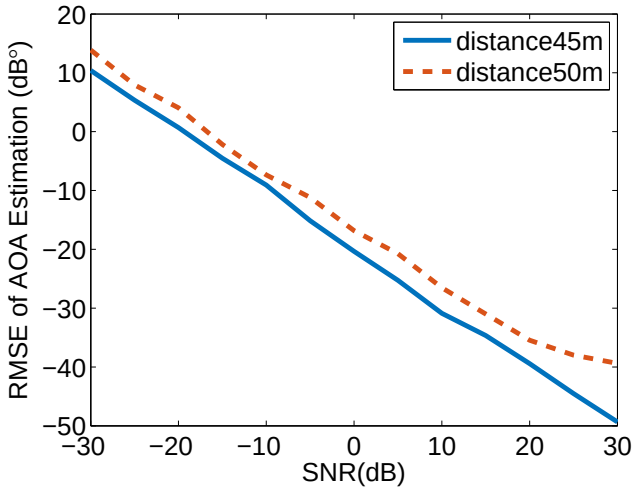


Fig. 19: RMSE of Case III.

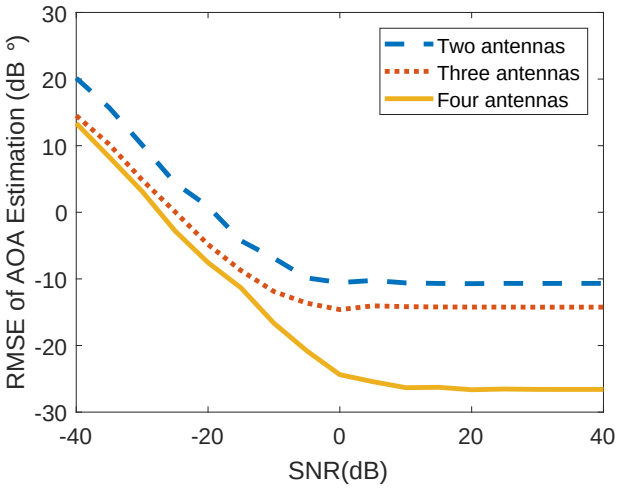


Fig. 20: RMSE of proposed algorithm with multi antennas.

performance of the proposed method can be further improved by increasing the number of receiver antennas.

## VI. Discussions

According to the definition of ultra-wideband (UWB), the wideband LFCMW signal considered in the paper can be regarded as one kind of UWB signals. The main difference between the proposed scheme and most UWB techniques is that most UWB techniques utilize the pulse signal while we consider the continuous LFCMW signal. To show the advantages of the proposed scheme, we illustrate the comparison between the proposed scheme and the pulse-based UWB technique in Table I according to [30]. The hardware complexity of both systems are similar. With the same bandwidth, the proposed scheme could achieve better accuracy and larger range since the signal is transmitted continuously which could effectively improve the SNR. Pulse-based UWB technique performs better when tracking moving targets benefiting from the high pulse repetition frequency [30].

| Category | Proposed Scheme | Pulse-based UWB |
|---|---|---|
| Accuracy | ✓ | |
| Hardware Complexity | - | - |
| Maximum Range | ✓ | |
| Track moving targets | | ✓ |

TABLE I: The comparison between the proposed scheme and pulse-based UWB [30].

## VII. Conclusion

In this paper, we have proposed a novel framework for estimating the AOA of multiple targets using wideband LFM-CW signal with only two receiver antennas. The proposed framework involves a preprocessing step to transform the wideband non-stationary signal into superposition of a series of single-tone signals. Signals reflected from different targets are separated using corresponding bandpass filters. Then the AOA of each target is estimated using the phase difference on the two receiver antennas. Theoretical analysis and simulation results demonstrate that the proposed framework can achieve accurate AOA estimation for multiple targets even at low SNR. Note that with two receiver antennas, the proposed method can only estimate the conic angle. However, with three receiver antennas, the proposed method can estimate both the azimuth and elevation angles.

## References

[1] Adib, F., Mao, H., Kabelac, Z., Katabi, D., Miller, R. C. "Smart homes that monitor breathing and heart rate," in *Proc. ACM CHI*, Apr. 2015, pp. 837-846.

[2] A. A. Winder, "II. Sonar system technology," *IEEE Trans. Sonics Ultrason.*, vol. SU-22, no. 5, pp. 291-32, Sep. 1975.

[3] J. R. Klauder, A. C. Price, S. Darlington, and W. J. Albersheim, "The theory and design of chirp radars," *Bell Syst. Tech. J.*, vol. 39, no. 4, pp. 745-808, Jul. 1960.

[4] R. Schmidt. "Multiple emitter location and signal parameter estimation," *IEEE Trans. Antennas Propag.*, vol. 34, no.3, pp. 276-280, Mar. 1986.

[5] M. A. Hasan, M. R. Azimi-Sadjadi, and A. A. Hasan, "Rational invariant subspace approximations with applications," *IEEE Trans. Signal Process.*, vol. 48, pp. 3032-3041, Nov. 2000

[6] M. Rubsamen and A. B. Gershman, "Direction-of-Arrival estimation for nonuniform sensor arrays: From manifold separation to fourier domain MUSIC methods," *IEEE Trans. Signal Process.*, vol. 57, pp. 588-599, Feb. 2009

[7] F. Yan, M. Jin and X. Qiao, "Low-Complexity DOA Estimation Based on Compressed MUSIC and Its Performance Analysis," *IEEE Trans. Signal Process.*, vol. 61, no. 8, pp. 1915-1930, April, 2013

[8] A. Paulraj, R. Roy, and T. Kailath, "A subspace rotation approach to signal parameter estimation," *IEEE Trans. Signal Process.*, vol. 74, pp. 1044-1046, Jul. 1986

[9] L. B. Almeida, "The fractional Fourier transform and time-frequency representations," *IEEE Trans. Signal Process.*, vol. 42, no. 11, pp.3084-3091, Nov. 1994.

[10] J. Yu, L.Zhang and K. Liu, "Coherently Distributed Wideband LFM Source Localization," *IEEE Signal Processing Lett.*, vol. 22, no.4, pp. 504-508, Apr. 2015.

[11] D. Liu, Z. Li, X. Guo and S. Zhao, "DOA estimation for wideband LFM signals with a few snapshots," *EURASIP J. WIREL. COMM.*, vol. 2017, pp. 28, Feb. 2017

[12] Ran Tao, Yunsong Zhou, "A novel method for the DOA estimation of wideband LFM sources based on FRFT," *J. Beijing Inst. Technol.*, vol. 25, pp. 895-899, October 2005.

[13] Haitao Qu, Lin Qi, Xiaomin Mu. "Estimation of coherent wideband LFM signals based on fractional Fourier domain," in *Proc. ICICIC*, Aug. 2006, pp. 18-21.

[14] X. Jin, T. Zhang, J. Bai and D. Zhao, "DOA estimation of coherent wideband LFM signals based on fractional fourier transform and virtual array," in *Proc. IEEE CISP*, Oct. 2010, pp. 4380-4384.

[15] H. Chong and Z. Xiaomin, "DOA estimation of multi-component LFM in complex environment using ESPRIT based on FRFT," in *Proc. ICSPCC*, Sept. 2011, pp. 1-4.
[16] A. Belouchrani and M. G. Amin, "Time-frequency MUSIC," *IEEE Signal Process. Lett.*, vol. 6, no. 5, pp. 109-110, May 1999.
[17] Y. Zhang, W. Mu, and M. G. Amin, "Subspace analysis of spatial time frequency distribution matrices," *IEEE Trans. Signal Process.*, vol. 49,no. 4, pp. 747-759, Apr. 2001.
[18] A. B. Gershman and M. G. Amin, "Wideband direction-of-arrival estimation of multiple chirp signals using spatial time-frequency distributions," *IEEE Signal Process. Lett.*, vol. 7, no. 6, pp. 152-155, Jun.2000.
[19] Yimin Zhang, B. A. Obeidat and M. G. Amin, "Spatial polarimetric time-frequency distributions for direction-of-arrival estimations," *IEEE Trans. Signal Process.*, vol. 54, no. 4, pp. 1327-1340, April 2006.
[20] Ning Ma and Joo Thiam Goh, "Ambiguity-function-based techniques to estimate DOA of broadband chirp signals," *IEEE Trans. Signal Process.*, vol. 54, no. 5, pp. 1826-1839, May 2006.
[21] T. D. Abhayapala and H. Bhatta, "Coherent broadband source localization by modal space processing," in *IEEE ICT* Feb. 2003, pp. 1617-1623
[22] D. Oh, Y. Ju, H. Nam and J. H. Lee, "Dual smoothing DOA estimation of two-channel FMCW radar," *IEEE Trans. Aerosp. Electron. Syst.* , vol. 52, no. 2, pp. 904-917, April 2016.
[23] A. Goldsmith, *Wireless Communication*. Cambridge University Press, 2005.
[24] A. G. Stove "Linear FMCW radar techniques" *IEE Proc. F(Radar and Signal Processing)*, vol. 139, no. 5, pp. 343-350, Oct. 1992
[25] Adriano Meta, Peter Hoogeboom and Leo P. Ligthart "Signal Processing for FMCW SAR" *IEEE Trans. Geosci. Remote Sens.*, vol. 45, no. 11, pp. 3519-3532, Nov. 2007
[26] S. O. Rice, "Mathematical Analysis of Random Noise," *Bell Syst. Tech. J.,* vol.24, no.1 pp. 44-156. Jan. 1945.
[27] Mahafza, Bassem R., *Radar systems analysis and design using MATLAB*. CRC press, 2002.
[28] R. F. Pawula, S.O.Rice and J.H.Roberts, "Distribution of the phase angle between two vectors perturbed by Gaussian noise," *IEEE Trans. Commun.*, vol. 30, no. 8, pp. 1828-1841, Aug. 1982.
[29] John G. Proakis, *Digital Communications, Fourth edition*. McGraw-Hill Companies, 2001.
[30] A. Figueroa, B. AI-Qudsi, N. Joram and F. Ellinger. "Comparison of two-way ranging with FMCW and UWB radar systems.", in *Proc. IEEE WPNC*, Oct. 2016, pp. 1-6.

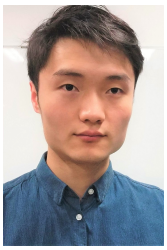

**Dongheng Zhang** received the B.S. degree from the School of Electronic and Engineering, University of Electronic Science and Technology of China, Chengdu, China, in 2017. He is currently pursuing the Ph.D. degree at the School of Information and Communication Engineering, University of Electronic Science and Technology of China. His research interests are in signal processing, wireless communications and networking.

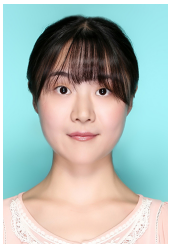

**Ying He** received the B.S. degree from the School of Electronic and Engineering, University of Electronic Science and Technology of China, Chengdu, China, in 2017. She is currently pursuing the Ph.D. degree at the School of Information and Communication Engineering, University of Electronic Science and Technology of China. Her research interests include wireless communications and signal processing.

**Xinyu Gong** is working toward his B.S in Computer Science from University of Electronic Science and Technology of China. His current research is on computer vision and deep learning.

**Yang Hu** received the B.S. and Ph.D. degrees in electrical engineering from the University of Science and Technology of China, Hefei, China, in 2004 and 2009 respectively. She was with the University of Maryland Institute for Advanced Computer Studies as a research associate from 2010 to 2015. She is currently an associate researcher with the School of Information and Communication Engineering at the University of Electronic Science and Technology of China, Chengdu, China. Her current research interests include computer vision, machine learning and multimedia signal processing.

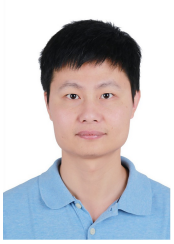

**Yan Chen** (SM'14) received the bachelor's degree from the University of Science and Technology of China in 2004, the M.Phil. degree from the Hong Kong University of Science and Technology in 2007, and the Ph.D. degree from the University of Maryland, College Park, MD, USA, in 2011. He was with Origin Wireless Inc. as a Founding Principal Technologist. Since Sept. 2015, he has been a full Professor with the School of Information and Communication Engineering at the University of Electronic Science and Technology of China. His research interests include multimedia, signal processing, game theory, and wireless communications.

He was the recipient of multiple honors and awards, including the best student paper award at the PCM in 2017, best student paper award at the IEEE ICASSP in 2016, the best paper award at the IEEE GLOBECOM in 2013, the Future Faculty Fellowship and Distinguished Dissertation Fellowship Honorable Mention from the Department of Electrical and Computer Engineering in 2010 and 2011, the Finalist of the Dean's Doctoral Research Award from the A. James Clark School of Engineering, the University of Maryland in 2011, and the Chinese Government Award for outstanding students abroad in 2010.

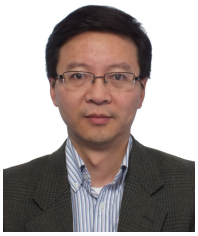

**Bing Zeng** (M'91-SM'13-F'16) received his BEng and MEng degrees in electronic engineering from University of Electronic Science and Technology of China (UESTC), Chengdu, China, in 1983 and 1986, respectively, and his PhD degree in electrical engineering from Tampere University of Technology, Tampere, Finland, in 1991.

He worked as a postdoctoral fellow at University of Toronto from September 1991 to July 1992 and as a Researcher at Concordia University from August 1992 to January 1993. He then joined the Hong Kong University of Science and Technology (HKUST). After 20 years of service at HKUST, he returned to UESTC in the summer of 2013, through Chinas 1000-Talent-Scheme. At UESTC, he leads the Institute of Image Processing to work on image and video processing, 3D and multi-view video technology, and visual big data.

During his tenure at HKUST and UESTC, he graduated more than 30 Master and PhD students, received about 20 research grants, filed 8 international patents, and published more than 260 papers. Three representing works are as follows: one paper on fast block motion estimation, published in IEEE Transactions on Circuits and Systems for Video Technology (TCSVT) in 1994, has so far been SCI-cited more than 1000 times (Google-cited more than 2200 times) and currently stands at the 8th position among all papers published in this Transactions; one paper on smart padding for arbitrarily-shaped image blocks, published in IEEE TCSVT in 2001, leads to a patent that has been successfully licensed to companies; and one paper on directional discrete cosine transform (DDCT), published in IEEE TCSVT in 2008, receives the 2011 IEEE CSVT Transactions Best Paper Award. He also received the best paper award at ChinaCom three times (2009 Xian, 2010 Beijing, and 2012 Kunming).

He served as an Associate Editor for IEEE TCSVT for 8 years and received the Best Associate Editor Award in 2011. He was General Co-Chair of VCIP-2016 and PCM-2017. He received a 2nd Class Natural Science Award (the first recipient) from Chinese Ministry of Education in 2014 and was elected as an IEEE Fellow in 2016 for contributions to image and video coding.